P3.19

Observational and Modeling Studies of Cloud and Associated Rainfall Processes

Xiaofan Li[1]
Joint Center for Satellite Data Assimilation and
NOAA/NESDIS/Office of Research and Applications, Camp Springs, Maryland

1. Observational Analysis

Water vapor is an important source for tropical convective development. It serves as the major constituent in moist available potential energy (Li et al. 2002c) and its horizontal gradient is more important than the horizontal temperature gradient so that the water-vapor gradient can replace equivalent potential gradient in the calculations in the new vorticity vectors (Gao et al. 2004, 2005b). As a critical atmospheric variable, its accurate simulation in numerical models may have important impacts on the cloud simulation.

The precipitable water (PW: the mass-integration of mixing ratio of water vapor) has been retrieved with satellite-measured radiances at NOAA/NESDIS/ Microwave Surface and Precipitation Products System (MSPPS), which is an operational product available to the public. To examine how well the numerical models simulate moisture patterns and magnitudes, the PW simulated by NOAA/NCEP/Global Data Assimilation System (GDAS) is validated with the satellite-retrieved PW. The patterns of PW in both simulation and satellite-retrieval are similar (not shown), which may be partially due to the inclusion of some observed moisture information in the GDAS. However, the magnitudes of PW in both simulation and satellite-retrieval could be different as indicated in Fig. 1 where the both data are averaged over the areas of 2^o by 2^o. The root-mean squared (RMS) differences of PW between simulation and satellite-retrieval are 2.5 mm over the clear-sky regions and 4.5 mm over cloudy regions (where IWP+LWP is larger than 0.0005 mm, IWP and LWP are the mass integrations of mixing ratios of water and ice hydrometeors, respectively). The standard derivations in MSPPS PW are 6.5 mm over the clear-sky regions and 6.0 mm over cloudy regions whereas those in GDAS are 6.4 mm over the clear-sky regions and 5.1 mm over cloudy regions. Both the RMS differences of PW between MSPPS and GDAS over clear-sky and cloudy regions are smaller than the standard deviations of PW whereas the RMS difference over clear-sky regions is smaller than that over cloudy regions, indicating that numerical model used in GDAS handles moisture simulation better over clear-sky regions than over cloudy regions. The area means in MSPPS PW are 42.3 mm over the clear-sky regions and 43.2 mm over cloudy regions whereas those in GDAS are 51.7 mm over the clear-sky regions and 52.1 mm over cloudy regions. Thus, the ratios of RMS difference to time mean (multiplying with 100 %) are 4.8-5.9 % over clear-sky regions and 8.4-10.2 % over cloudy regions. The simulated PW could be more than 10 % away from the satellite-retrieval over cloudy regions.

The MSPPS also retrieves IWP and LWP whereas the GDAS contains calculation of cloud profile, which can be used to compute IWP and LWP. However, Cumulus parameterization scheme and explicit cloud microphysical parameterization scheme are included in GDAS while that the condensation immediately leads to precipitation without the presence of clouds is assumed in the cumulus parameterization scheme. Thus, the water hydrometeors in the tropical calculations of the cumulus parameterization scheme are excluded in the GDAS calculations of LWP, which yields significantly smaller LWP (~ 0.5 mm) than that retrieved by MSPPS (~ 1-2 mm) (Fig. 2a). The magnitudes of IWP in both GDAS and MSPPS in Fig. 2b are similar (~ 1 mm), whereas their RMS difference is 0.12 mm. The standard deviations of IWP are 0.11 mm for MSPPS data and 0.06 mm for GDAS data. Thus, the RMS differences are larger than the standard deviations. The time means of IWP are 0.05 mm for MSPPS data and 0.04 mm for GDAS data. Thus, the ratios of RMS difference to time mean (multiplying with 100 %) are 222-300 %. These results indicate that the cloud simulations in GDAS may not be skillful.

2. Cloud-resolving simulations

The cloud-resolving model used in this study (Tao and Simpson 1993) includes five prognostic equations for mixing ratios of cloud water, raindrop, cloud ice, snow, and graupel, the cloud microphysical parameterization schemes, solar and thermal infrared radiation parameterization schemes. Cyclic lateral boundaries are used. The horizontal domain is 768 km with a horizontal grid resolution of 1.5 km. The top model level is 42 mb. The vertical grid resolution ranges from about 200 m near the surface to about 1 km near 100 mb. The time step is 12 s. Hourly zonal-mean simulation data are used in the following analysis. The cloud-resolving simulations have been validated with observations in terms of atmospheric thermodynamic profiles, surface fluxes, and surface rain rate in the tropics during the Global Atmospheric Research Program Atlantic Tropical Experiment (GATE) (e.g., Xu and Randall 1996; Grabowski et al. 1996) and TOGA COARE (e.g., Wu et al. 1998; Li et al. 1999, 2002a, b, c, 2004; Gao et al. 2004, 2005a, b).

---

[1] Corresponding author address: Xiaofan Li, JCSDA and NOAA/NESDIS/ORA, 5200 Auth Road, Room 712, Camp Springs, MD 20746 Email: Xiaofan.Li@noaa.gov

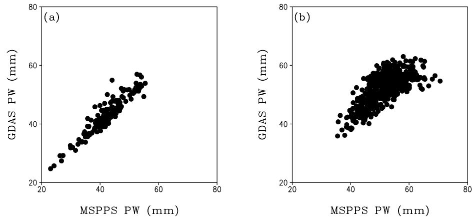

Fig. 1 GDAS PW versus MSPPS PW in (a) clear-sky regions and (b) cloudy regions based on the data with the horizontal resolution of 2^o x 2^o. Unit is in mm.

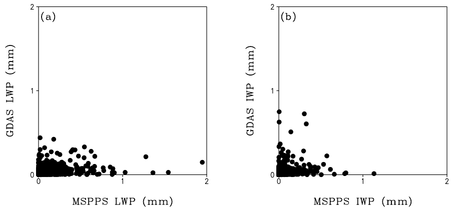

Fig. 2 GDAS LWP versus MSPPS LWP in (a) and GDAS IWP versus MSPPS IWP in (b) based on the data with the horizontal resolution of 2^o x 2^o.. Unit is in mm.

The model is forced by zonally-uniform vertical velocity, zonal wind, along with thermal and moisture advection based on 6-hourly GDAS data averaged over 150-160^{o}E, EQ. Daily-mean sea surface temperature (SST) data are retrieved from NASA/TRM TMI radiometer with a 10.7 GHz channel (Wentz et al. 2000), which are also imposed in the model. The model is integrated from 1100 LST 18 to 1700 LST 26 April 2003 (8.25 days total). Figure 3 shows the time evolution of the vertical distribution of the large-scale vertical velocity and zonal wind, which are imposed in the model during the integrations. The ascending motion with maximum of – 4 mb h^{-1} occurs around 300 mb on 18 April 2003. Moderate upward motions of –2 mm h^{-1} appear daily in mid and lower troposphere from 20 to 22 April when westerly winds confine in the lower troposphere while easterly winds weaken gradually. Two strong ascending motion centers extend from the lower troposphere to the upper troposphere on 24 and 25 April when the westerly winds switch into the intensified easterly winds. Three experiments are designed. Experiment C is a control experiment. Experiment CP and CM are identical to experiment C except that 10 % of PW is added and reduced in CP and CM, respectively, while the vertical structures of specific humidity are kept.

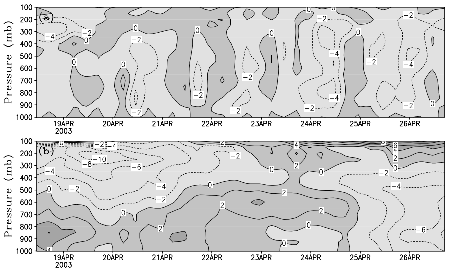

Fig. 3 Temporal and vertical distributions of (a) vertical velocity (mb h^{-1}) and (b) zonal wind (m s^{-1}) obtained from GDAS for a selected 8-day period.

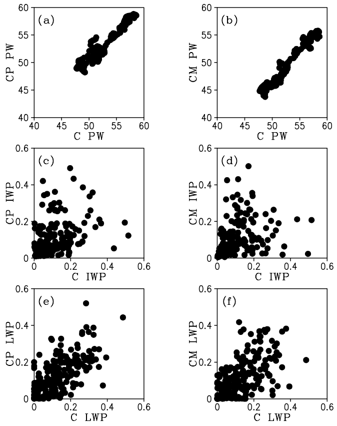

Fig. 4 CP versus C for (a) PW, (c) IWP, (e)LWP, and CM versus C for (b)PW, (d)IWP, (f)LWP. Unit is in mm.

The scatter plotting of CP versus C and CM versus C for PW, IWP, and LWP is shown in Fig. 4. The PW simulated in CP and C is along the diagonal line of the diagram, indicating a small RMS difference (1.1 mm), although the initial difference in PW is 5.1 mm. The PW simulated in CM and C is below the diagonal line of the diagram, suggesting a large RMS difference (3.3 mm). The ratios of RMS difference to time mean of PW (multiplying with 100 %) are 2.1 % in CP n 6.6 % in CM. The RMS difference between CP and C is much smaller than the standard deviation of CP (3.3 mm) whereas that between CM and C is marginally smaller than the standard deviation of CM (3.8 mm).

Cloud hydrometeors (LWP and IWP) simulated in CP and CM versus those simulated in C show large scatter patterns that are away from the diagonal lines (Fig. 4c-f). The RMS difference in IWP between CP and C is 0.104 mm whereas that between CM and C is 0.107 mm, which is larger than the standard deviations of CP (0.094 mm) and CM (0.093 mm). The ratios of RMS difference to time mean of IWP (multiplying with 100 %) are 99 % in CP and 102 % in CM. The small initial difference in PW produces the large difference in IWP. This demonstrates that the large RMS difference in IWP between MSPPS and GDAS may be caused by the small RMS difference in PW. The large scattering in IWP between CP/CM and C associated with the small scattering in PW implies uncertainties in cloud microphysical parameterization schemes that are nonlinear functions of temperature and moisture.

The RMS difference in LWP between CP and C is 0.085 mm whereas that between CM and C is 0.096 mm, which are smaller than the standard deviations of CP (0.098 mm) and CM (0.103 mm). The ratios of RMS difference to time mean of LWP (multiplying with 100 %) are 86.7 % in CP and 93.2 % in CM, which are smaller than those of IWP.

Following Gao et al. (2005a), zonal-mean surface rain rate (P_s) can be symbolically expressed as

$$P_s = Q_{WVT} + Q_{WVF} + Q_{WVE} + Q_{CM}\,, \qquad (1)$$

$$Q_{WVT} = -\frac{\partial [q_v]}{\partial t}\,; \quad Q_{WVF} = -[\bar{u}^o \frac{\partial \bar{q}_v{}^o}{\partial x}] - [\bar{w}^o \frac{\partial \bar{q}_v}{\partial z}]\,;$$

$Q_{WVE} = E_s$; $Q_{CM} = -\frac{\partial [q_5]}{\partial t}$; Q_{WVF} is vapor convergence, which is mainly contributed by vertical advective moistening/drying since imposed horizontal vapor advection is much smaller than the vertical advection; q_v is specific humidity; u and w are zonal and vertical wind components, respectively; Q_{WVE} is surface evaporation rate; $q_5 = q_c + q_r + q_i + q_s + q_g$, q_c, q_r, q_i, q_s, q_g are the mixing ratios of cloud water (small cloud droplets), raindrops, cloud ice (small ice crystals), snow (density 0.1 g cm^{-3}), and graupel (density 0.4 g cm^{-3}), respectively; $-[u\frac{\partial q_5}{\partial x}] - [w\frac{\partial q_5}{\partial z}] = 0$ due to cyclic boundary conditions; Overbar denotes a zonal-mean; [ ] is a zonal-mean mass integration; superscript ^{o} is an imposed observed value.

Surface rain rates simulated in CP and CM versus those simulated in C also show a large scatter pattern (Fig. 5a,b). The RMS difference in P_s between CP and C is 0.28 mm h^{-1} whereas that between CM and C is 0.33 mm h^{-1}, which are similar to the standard deviations of CP (0.29 mm) and CM (0.32 mm). The ratios of RMS difference to time mean of P_s (multiplying with 100 %) are 89.6 % in CP and 110 % in CM. Although the large-scale ascending motion is imposed in the model, the small difference in PW still produces the large difference in the surface rain rate.

Q_{WVT} and Q_{CM} display large scatter patterns between CP/CM and C whereas Q_{WVF} and Q_{WVE} show good relationships between CP and C, and CM and C. The RMS differences in Q_{WVF} (~0.01 mm h^{-1}) and Q_{WVE} (~0.02 mm h^{-1}) are significantly smaller than the standard deviations of CP (0.24 mm h^{-1}) and CM (0.04 mm h^{-1}), respectively. The small RMS difference in Q_{WVF} reflects the dominance of imposed vertical velocity during the integrations. The RMS differences in Q_{WVT} between CP and C (0.37 mm h^{-1}) and CM and C (0.4 mm h^{-1}) are larger than the standard deviations of CP (0.32 mm h^{-1}) and CM (0.3 mm h^{-1}), respectively, whereas The RMS differences in Q_{CM} between CP and C (0.27 mm h^{-1}) and CM and C (0.29 mm h^{-1}) are larger than the standard deviations of CP (0.19 mm h^{-1}) and CM (0.19 mm h^{-1}), respectively. This indicates that the RMS differences in Q_{WVT} and Q_{CM} largely contribute to the RMS differences in P_s.

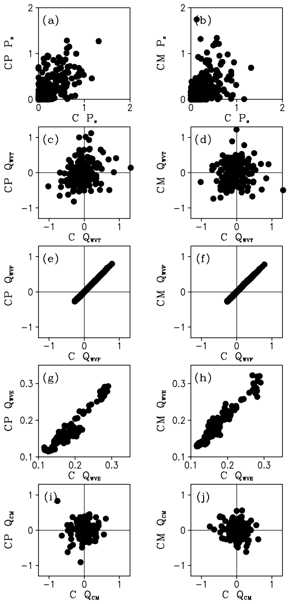

Fig. 5 CP versus C for (a) P_s, (c) Q_{WVT}, (e) Q_{WVF}, (g) Q_{WVE}, (i) Q_{CM} and CM versus C for (b) P_s, (d) Q_{WVT}, (f) Q_{WVF}, (h) Q_{WVE}, (j) Q_{CM}. Units are in mm h^{-1}.

To explain the large RMS differences in Q_{WVT} and Q_{CM}, the vertically-integrated water vapor and total cloud budgets will be analyzed. Following Sui et al. (2005), the vertically-integrated water vapor and total cloud budgets can be, respectively, expressed as

$$Q_{WVT} + Q_{WVF} + Q_{WVE} = P_{CND} + P_{DEP} + P_{SDEP} + P_{GDEP} - P_{REVP} - P_{MLTS} - P_{MLTG}\,, \qquad (2a)$$

$$Q_{CM} = P_s - P_{CND} - P_{DEP} - P_{SDEP} - P_{GDEP} + P_{REVP} + P_{MLTS} + P_{MLTG}\,, \qquad (2b)$$

where $[P_{CND}]$+ $[P_{DEP}]$+ $[P_{SDEP}]$+ $[P_{GDEP}]$ represents the sink term in moisutre budget that consists of vapor condensation rate ($[P_{CND}]$), vapor deposition rates for growth of cloud ice ($[P_{DEP}]$), snow ($[P_{SDEP}]$), and graupel ($[P_{GDEP}]$), and $[P_{REVP}]$+ $[P_{MLTS}]$+ $[P_{MLTG}]$ represents the source term consisting of growth of vapor by evaporation of raindrop ($[P_{REVP}]$), melting snow ($[P_{MLTS}]$), and melting graupel ($[P_{MLTG}]$).

Figure 6 shows scatter diagrams of CP versus C and CM versus C for $[P_{CND}]$, $[P_{DEP}]$, $[P_{SDEP}]$, $[P_{GDEP}]$, $[P_{REVP}]$, $[P_{MLTS}]$, and $[P_{MLTG}]$. The standard deviations of $[P_{CND}]$ (~0.36 mm h^{-1}) is much larger than those of $[P_{DEP}]$, $[P_{SDEP}]$, $[P_{GDEP}]$, $[P_{REVP}]$, $[P_{MLTS}]$, and $[P_{MLTG}]$ (~0.06-0.12 mm h^{-1}), indicating a large fluctuation of vapor condensation rate. The RMS differences in $[P_{DEP}]$ between CP and C (0.38 mm h^{-1}) and CM and C (0.41 mm h^{-1}) are larger than the standard deviations. Thus, vapor condensational process is responsible for the large RMS differences in Q_{WVT}, Q_{CM}, and P_s.

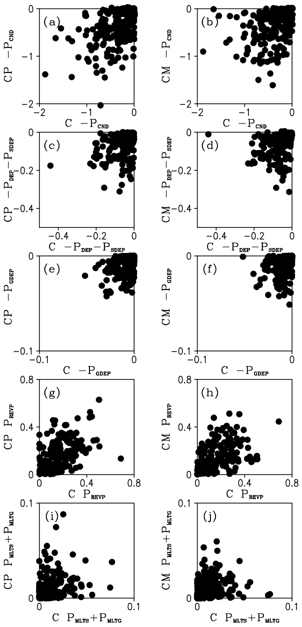

Fig. 6 CP versus C for (a) -$[P_{CND}]$, (c) -$[P_{DEP}]$-$[P_{SDEP}]$, (e) -$[P_{GDEP}]$, (g) $[P_{REVP}]$, (i) $[P_{MLTS}]$+$[P_{MLTG}]$ and CM versus C for (b) -$[P_{CND}]$, (d) -$[P_{DEP}]$-$[P_{SDEP}]$, (f) -$[P_{GDEP}]$, (h) $[P_{REVP}]$, (j) $[P_{MLTS}]$+$[P_{MLTG}]$. Units are in mm h^{-1}.

References

Gao, S., F. Ping, X. Li, and W.-K. Tao, 2004: A convective vorticity vector associated with tropical convection: A 2D cloud-resolving modeling study. *J. Geophys. Res.*, **109**, D14106, doi: 10.1029/2004JD004807.

Gao, S., X. Cui, Y. Zhu, and X. Li, 2005a: Surface rainfall processes as simulated in a cloud resolving model. *J. Geophys. Res.*, **110**, D10202, doi: 10.1029/2004JD005467.

Gao, S., X. Cui, Y. Zhou, X. Li, and W.-K. Tao, 2005b: A modeling study of moist and dynamic vorticity vectors associated with 2D tropical convection. *J. Geophys. Res.*, **110**, D17104, doi:10.1029/2004JD005675.

Grabowski, W. W., X. Wu, and M. W. Moncrieff, 1996: Cloud-resolving model of tropical cloud systems during Phase III of GATE. Part I: Two-dimensional experiments. *J. Atmos. Sci.*, **53**, 3684-3709.

Li, X., C.-H. Sui, K.-M. Lau, and M.-D. Chou, 1999: Large-scale forcing and cloud-radiation interaction in the tropical deep convective regime. *J. Atmos. Sci.*, **56**, 3028-3042.

Li, X., C.-H. Sui, and K.-M. Lau, 2002a: Precipitation efficiency in the tropical deep convective regime: A 2-D cloud resolving modeling study. *J. Meteor. Soc. Japan*, **80**, 205-212.

Li, X., C.-H. Sui, and K.-M. Lau, 2002b: Dominant cloud microphysical processes in a tropical oceanic convective system: A 2-D cloud resolving modeling study. *Mon. Wea. Rev.*, **130**, 2481-2491.

Li, X., C.-H. Sui, and K.-M. Lau, 2002c: Interactions between tropical convection and its environment: An energetics analysis of a 2-D cloud resolving simulation. *J. Atmos. Sci.*, **59**, 1712-1722.

Li, X., C.-H. Sui, K.-M. Lau, and W.-K. Tao, 2004: Tropical convective responses to microphysical and radiative processes: A 2D cloud-resolving modeling study. *Meteor. Atmos. Phys.*, doi: 10.1007/s00703-004-0088-5.

Sui, C.-H., X. Li, M.-J. Yang, and H.-L. Huang, 2005: Estimation of oceanic precipitation efficiency in cloud models. *J. Atmos. Sci.*, In press.

Tao, W.-K., and J. Simpson, 1993: The Goddard Cumulus Ensemble model. Part I: Model description. *Terr. Atmos. Oceanic Sci.*, **4**, 35-72.

Wentz, F. J., C. Gentemann, D. Smith, D. Chelton, 2000: Satellite measurements of sea surface temperature through clouds. *Science*, **288**, 847-850.

Wu, X., W. W. Grabowski, and M. W. Moncrieff, 1998: Long-term evolution of cloud systems in TOGA COARE and their interactions with radiative and surface processes. Part I: Two-dimensional cloud-resolving model. *J. Atmos. Sci.*, **55**, 2693-2714.

Xu, K.-M., and D. A. Randall, 1996: Explicit simulation of cumulus ensembles with the GATE Phase III data: Comparison with observations. *J. Atmos. Sci.*, **53**, 3710-3736.